Auxiliary Material

The Auxiliary Material for this article presents additional figures that illustrate the validity of our final model (Figure 6). In the first section we display ray-tracing diagrams and data panels. The ray diagrams show which portions of the model space are constrained by travel times from these individual data records. The data panels illustrate how the data misfit varies with source-receiver offset. In the second section we illustrate the modeling uncertainties and trade-offs between model parameters in our final solution.

1. Ray-tracing diagrams.

The summary figure of all ray paths and travel-time fits (Figure 7) gives an impression of the data coverage, but it does not illustrate well how individual OBS data records provide constraints on different parts of the model. We therefore display data panels with travel-time misfit and ray-tracing diagrams for 11 instruments along line SERP (Figure S1 to S11). In each of these figures, the data are shown with a reduction velocity of 7 km/s (top panels). The solid lines represent travel-time picks, the dashed lines are travel-time fits for the seismic velocity model of Figure 6. The phases that we identified are crustal turning waves Pg (blue), of mid-crustal reflections PiP (yellow), lower crustal refractions (purple), Moho reflections PmP (green), and mantle turning waves Pn (red). Ray paths in the seismic velocity model of Figure 6 (bottom panels) for each of these phases are shown in the same color. Gray lines drawn on the final velocity model indicate the seafloor, top of basement, a mid-crustal boundary, and Moho.

Refractions from the SERP airgun shots are recorded by OBS 2 only at source-receiver offsets less than 50 km (Figure S1), but they include mid-crustal reflections (yellow). The data of OBS 4 (Figure S2) show that R/V *Marcus Langseth* airgun shots between 270 and 295 km were very weak or missing due to a shutdown of the operations in the presence of sea turtles. The refractions from OBS 6 (Figure S3) and OBS 9 (Figure S4) show that mantle arrivals (red) are recorded over longer offsets in the central and northwestern portion of SERP than to the southeast. All OBSs on the EPR segment (Figure S4 to S11) sample mantle seismic velocities that are clearly less than 8 km/s at source-receiver offsets between 30 km and 70 km. However, OBS 11 (Figure S5), OBS 12 (Figure S6), OBS 13 (Figure S7), and OBS 14 (Figure S8), and OBS 17 (Figure S10) sample at least some 8.0 km/s mantle seismic velocities at larger source-receiver distances. The combined inversion of these seismic arrival times resulted in our model of Figure 6.

2. Model Covariance

The resolution test for our final seismic velocity model (Figure 9) quantifies the degree of spatial smoothing of seismic structure. A different measure of the quality of our inversion result is the a posteriori covariance between model parameters [*Menke*, 1984]. The diagonal of this matrix contains the variance of each model parameter in the inversion, and the off-axis elements represent the trade-off between two different model parameters.

To measure uncertainties in crustal and mantle seismic velocities and Moho depth in our model, we calculate model covariance in the EPR segment (Figure S12). At 130 km in our SERP model, the standard deviation in Moho depth is estimated to be 1.3 km (Figure S12b). This uncertainty is quite large considering that the laterally uniform EPR oceanic crust of approximately 6 km thickness in our model is in good agreement with seismic velocity models for other OBS seismic refraction profiles in the vicinity [*Christeson et al.,* 1999; *Walther et al.,* 2000; *Grevemeyer et al.,* 2007; *Ivandic et al.,* 2008]. This uncertainty therefore does not affect our interpretation. Moreover, the trade-off between these Moho depth nodes and nearby seismic velocity nodes is quite small (Figure S12b). The model covariance for seismic velocity nodes in the mantle (Figure S12c and Figure S12d) shows that the standard deviation in well-covered portions of the mantle is typically less than 0.1 km/s. The negative covariance between high-velocity anomaly Q and low-velocity anomalies R (Figure S12) clearly results from the trade-off between data misfit and model roughness in our linearized inversion. If we apply more smoothing in the inversion we will obtain more homogenous structure, so the seismic velocity at Q will decrease, whereas it will increase at R. On the other hand, if we relax the smoothing the seismic velocity at Q will increase, and it will decrease at R. The smoothness constraints in our tomographic inversion make us underpredict the magnitude of seismic velocity anomalies, but given that all trade-off estimates (Figure S12) are below 0.1 km/s we consider our conclusions to be warranted by the data.

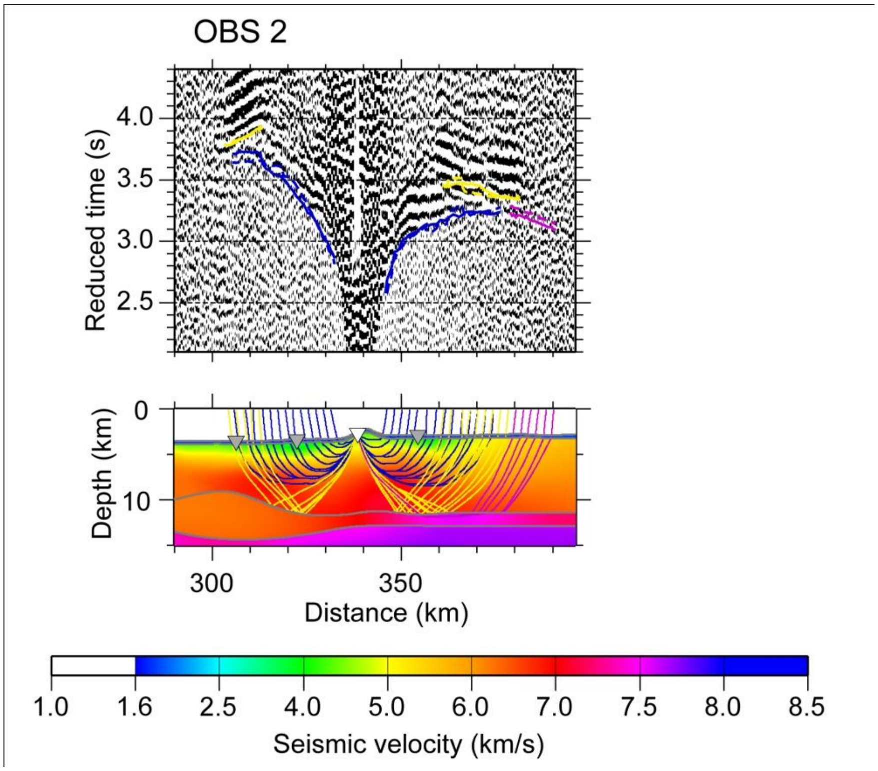

Figure S1. Data record and ray diagram for OBS 2.

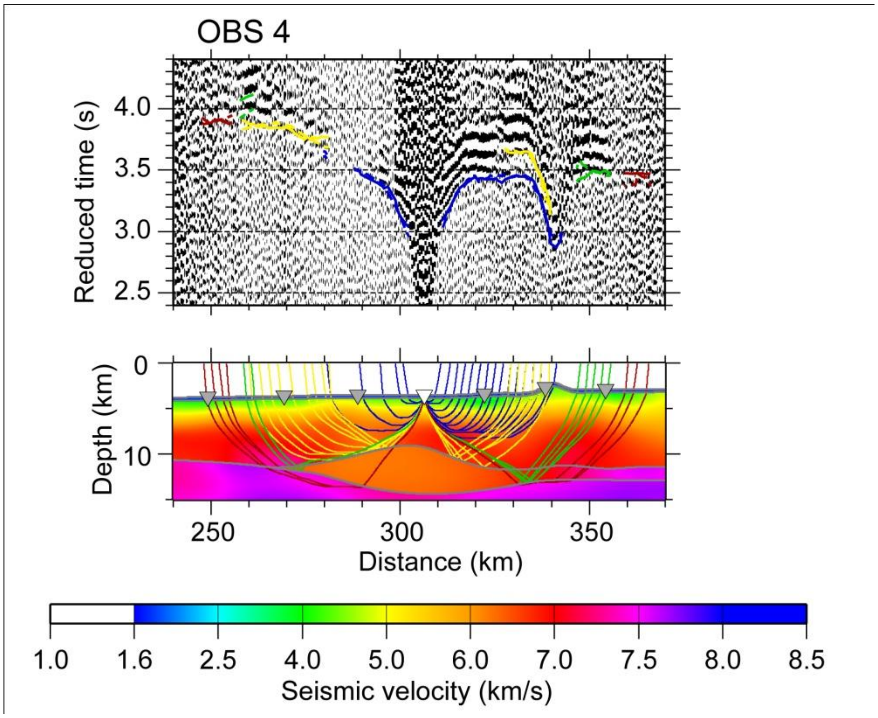

Figure S2. Data record and ray diagram for OBS 4.

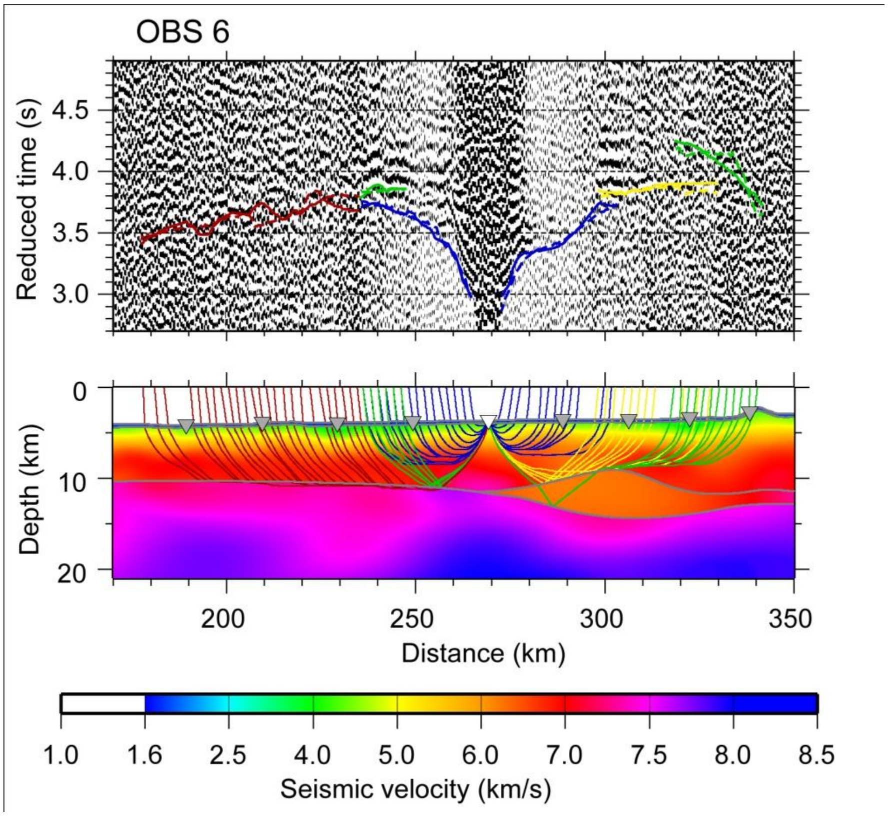

Figure S3. Data record and ray diagram for OBS 6.

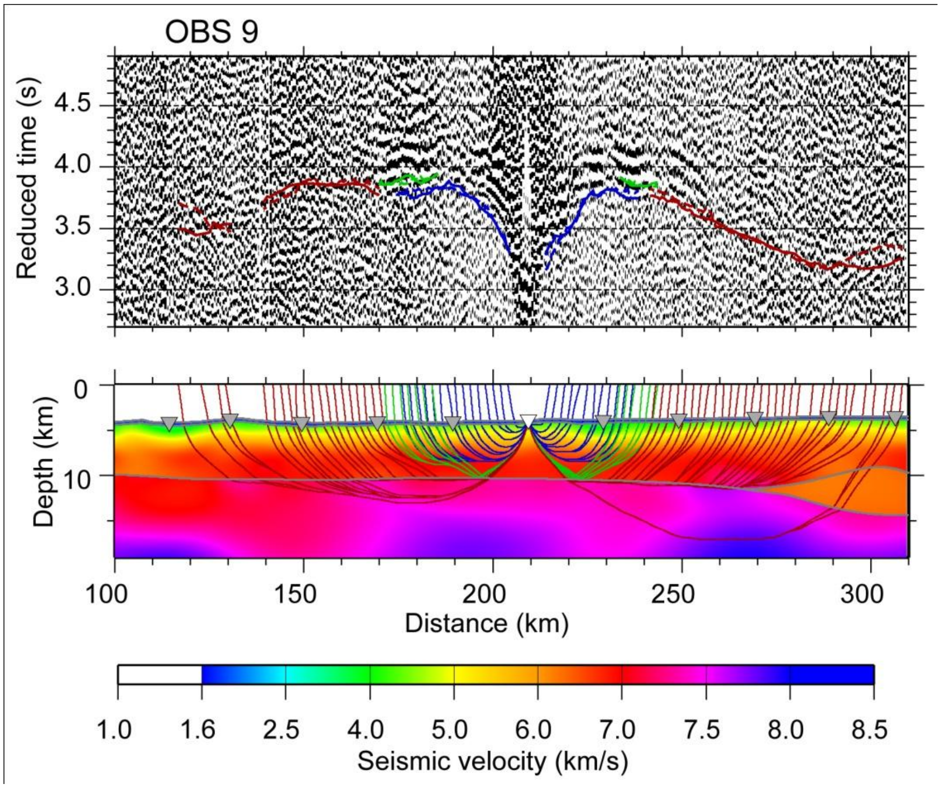

Figure S4. Data record and ray diagram for OBS 9.

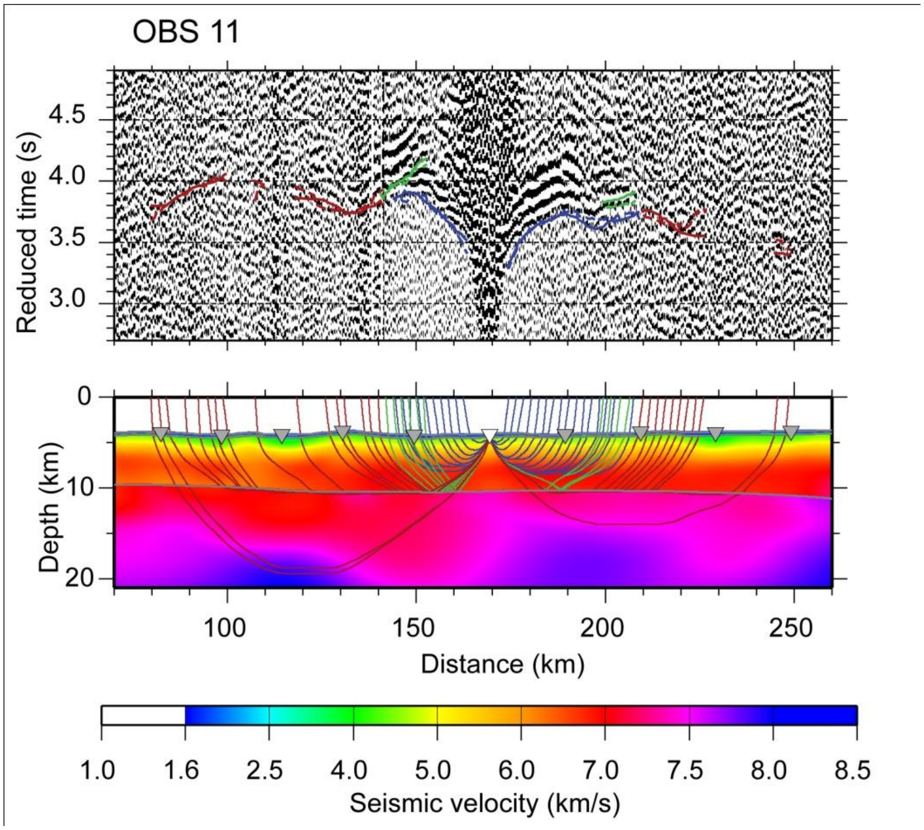

Figure S5. Data record and ray diagram for OBS 11.

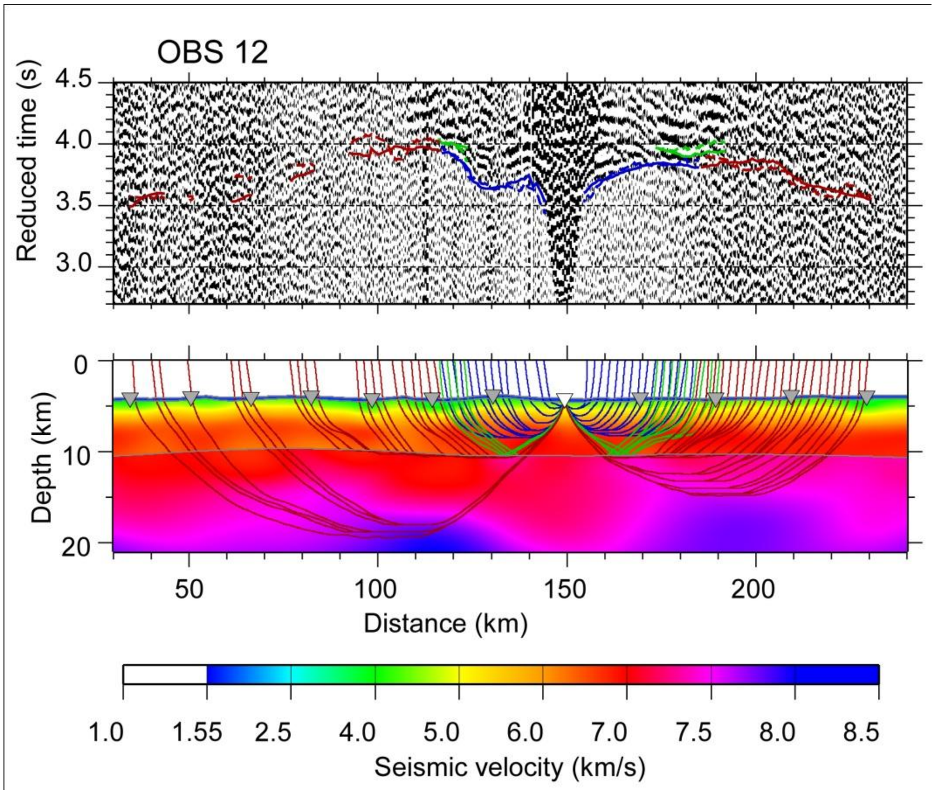

Figure S6. Data record and ray diagram for OBS 12.

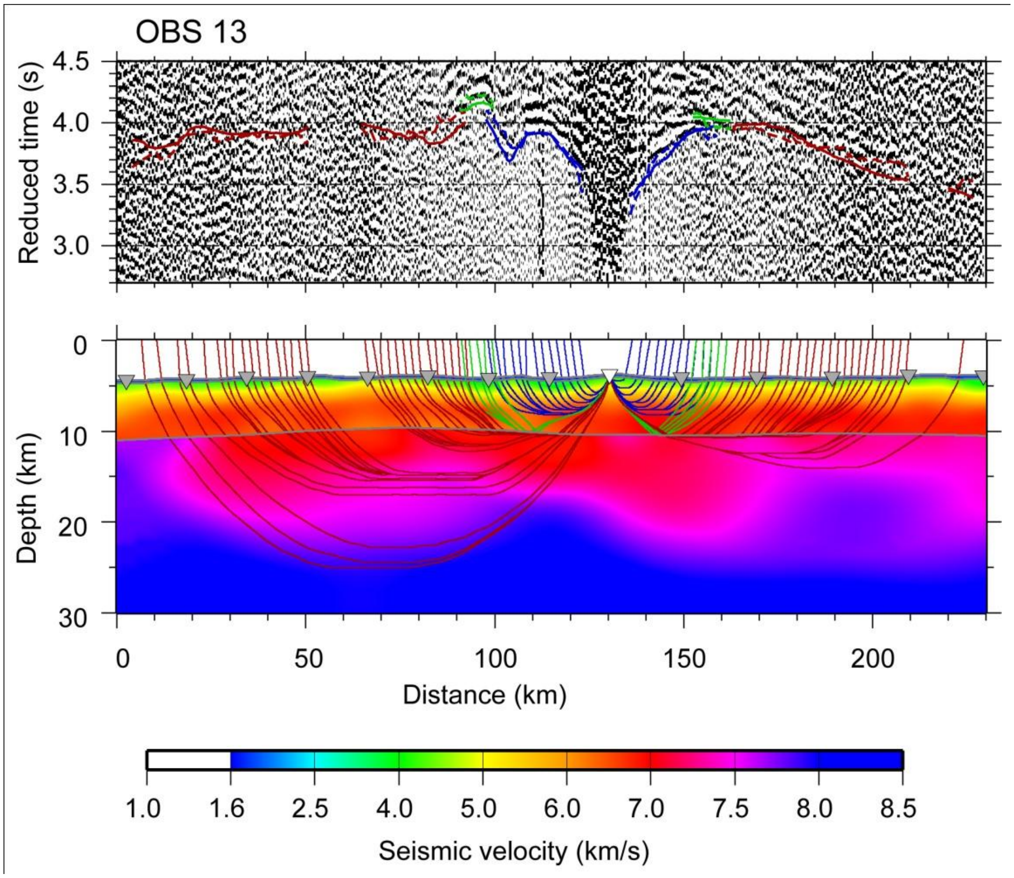

Figure S7. Data record and ray diagram for OBS 13.

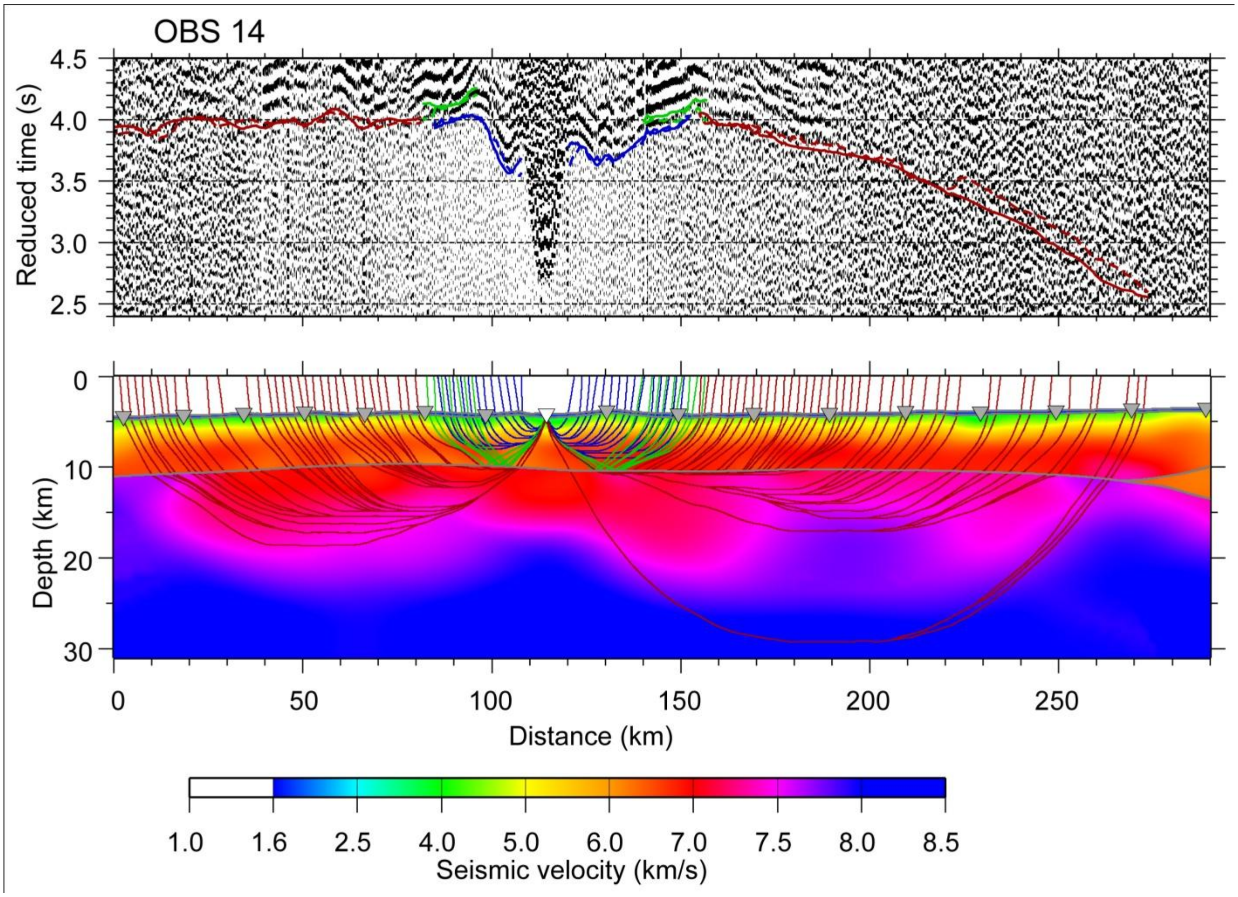

Figure S8. Data record and ray diagram for OBS 14.

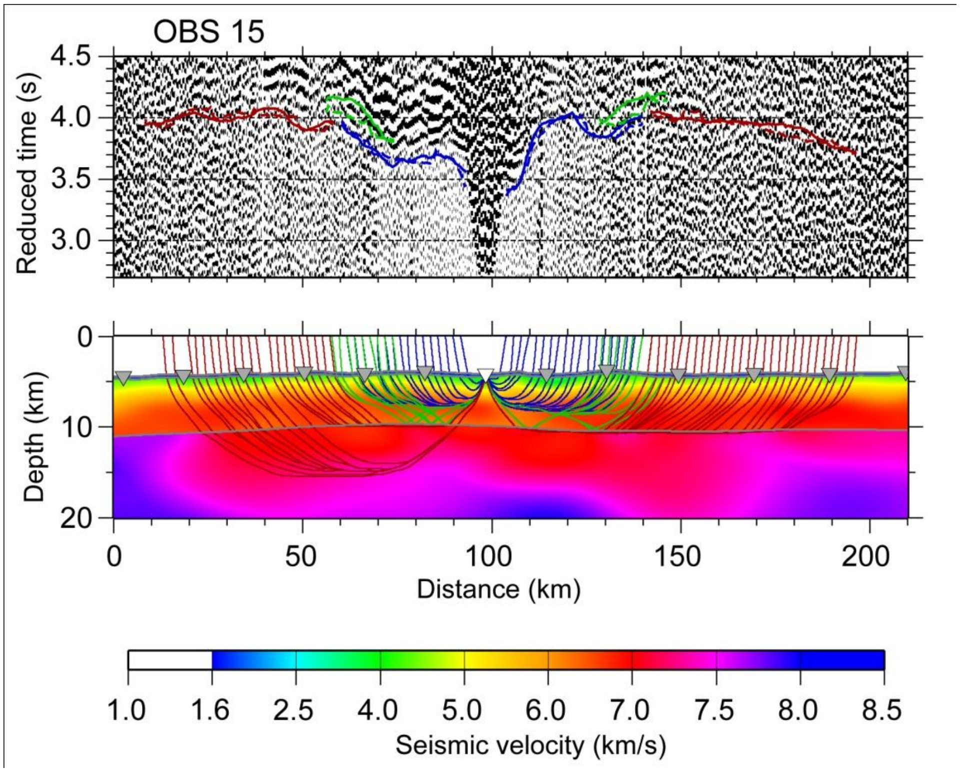

Figure S9. Data record and ray diagram for OBS 15.

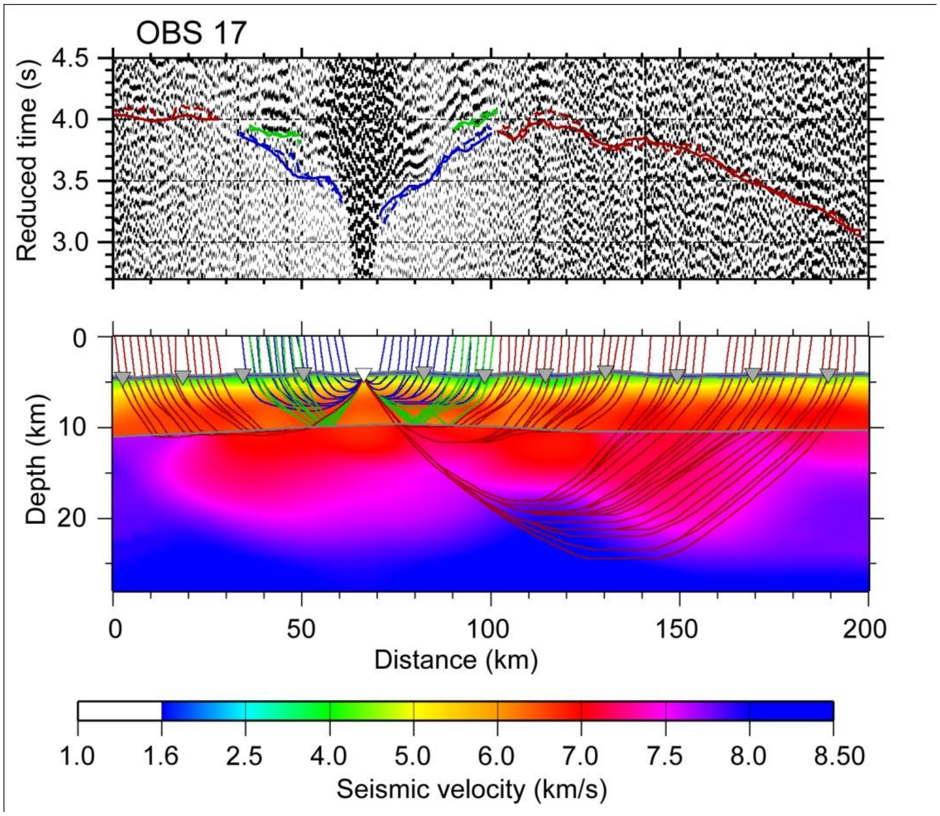

Figure S10. Data record and ray diagram for OBS 17.

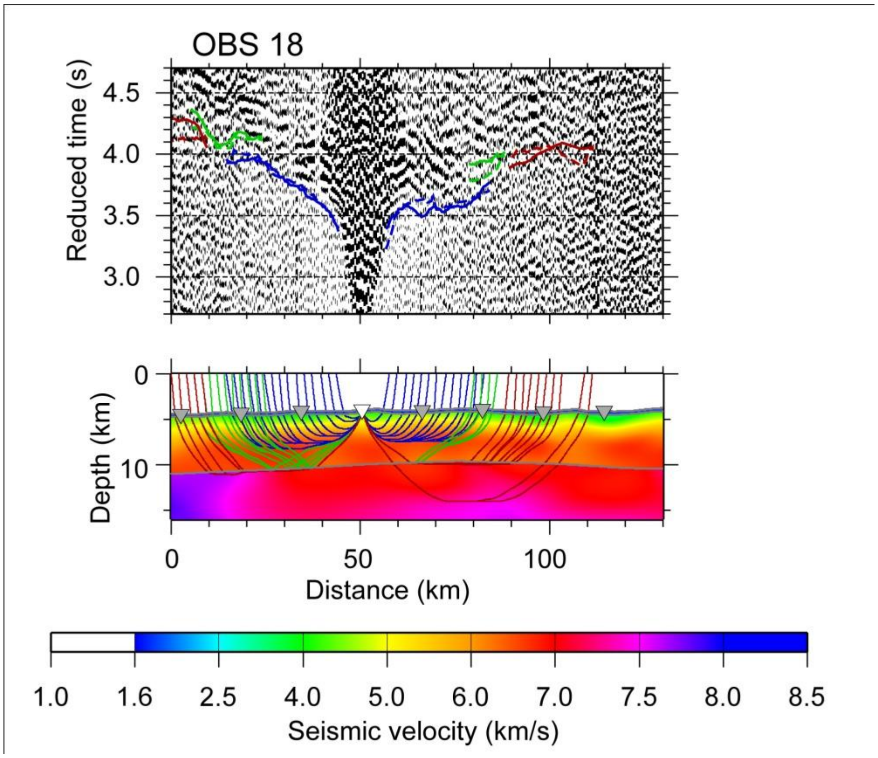

Figure S11. Data record and ray diagram for OBS 18.

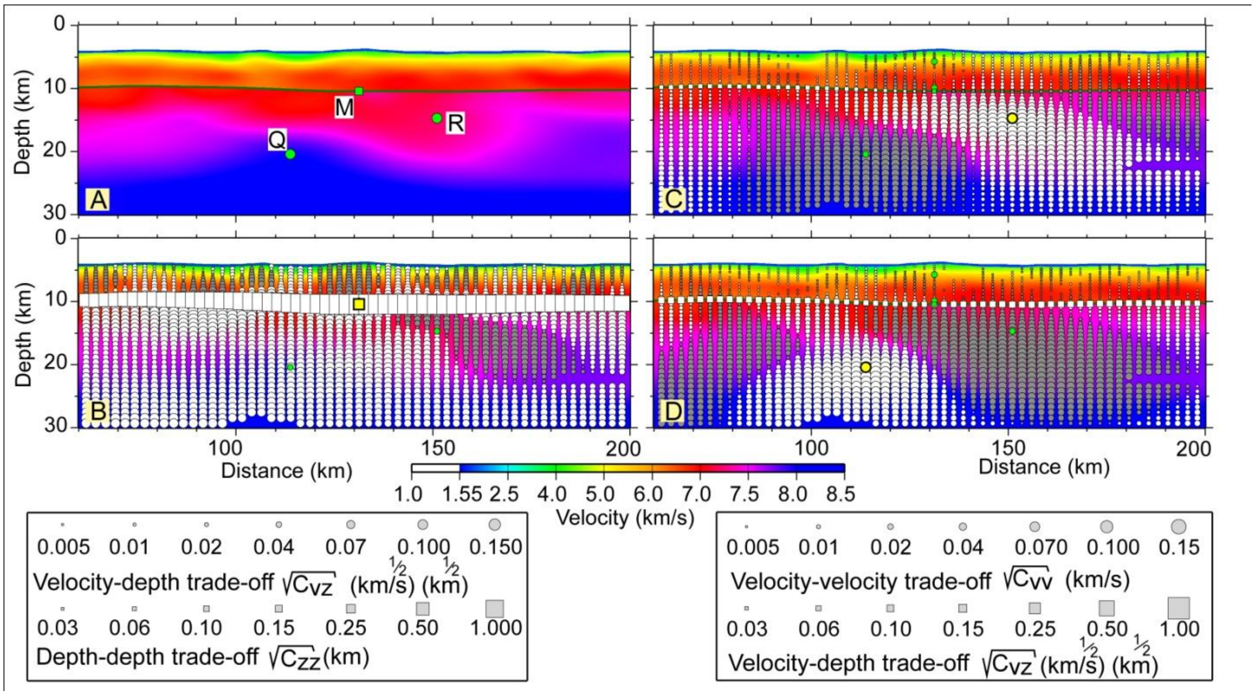

Figure S12. A posteriori model covariance [*Menke*, 1984] for the final seismic velocity model (Figure 6). a) Trade-off between three model parameters (Q, R, and M) and the SERP model between 60 km and 200 km. The first two parameters are velocity grid node in the mantle, whereas M is a Moho depth parameter. In each panel, velocity nodes are marked with circles, depth nodes are marked with squares. b) Square root of the covariance between M (yellow square) and the surrounding model space. Positive covariance is shown in white, and negative covariance appears in gray. The size of symbols indicates the magnitude of the covariance with M. The scale for depth-velocity (C_{vz}) and depth-depth (C_{zz}) covariance with M is shown in the left legend box. c) Covariance between R (yellow circle) and other model parameters. The scale for velocity-velocity (C_{vv}) and velocity-depth (C_{vz}) covariance is shown in the right legend box. d) Covariance between Q (yellow circle) and other model parameters.